International Tables for Crystallography (2006). Vol. C, Section 2.3.1.1.6, pp. 48–49.

published by Wilson (1963, 1974). His work provides the mathematical foundation for understanding the origin and treatment of the various sources of errors. The major aberrations are described in the following and are illustrated with experimental profiles and plots of computed data for better visualization and interpretation of the effects. The information can be used to correct the experimental data, interpret the profile broadening and shifts, and evaluate the precision of the analysis. Chapter 5.2 contains tables listing the centroid displacements and variances of the various aberrations.

The magnitudes of the aberrations and their effects are illustrated in Figs. 2.3.1.8(*a*) and (*b*), which show the Cu $K\alpha_1, K\alpha_2$ spectrum inside the experimental profile. At high 2θ's, the shape of the experimental profile is largely determined by the spectral distribution, but at low 2θ's the aberrations are the principal contributors. The basic experimental high-resolution profile shapes from specimens without appreciable broadening effects (NIST silicon powder standard) are shown in Figs. 2.3.1.8(*c*)–(*f*). The solid-line profiles were obtained with a reflection specimen (Fig. 2.3.1.3), and the dashed-line profiles with transmission-specimen geometry (Fig. 2.3.1.12). The differences in the $K\alpha_1, K\alpha_2$ doublet separations are explained in Subsection 2.3.1.2. These profiles are the basic instrument functions which show the profile shapes contained in all reflections recorded with these methods. The shapes are modified by changing slit sizes.

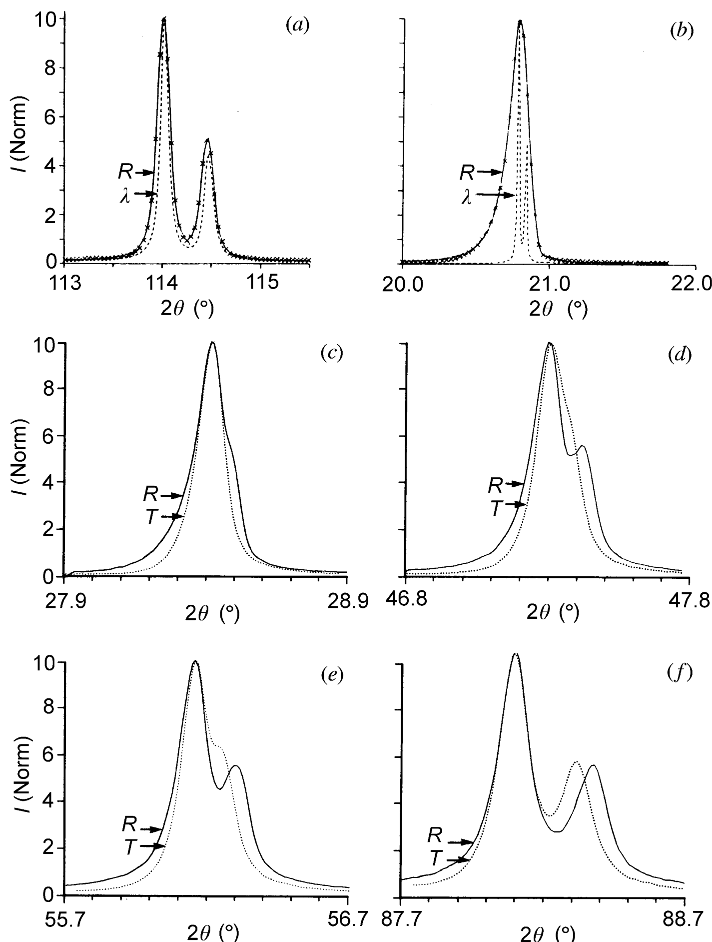

Fig. 2.3.1.8. Diffractometer profiles. (*a*) and (*b*) Spectral profiles λ of Cu $K\alpha$ doublet (dashed-line profiles) inside experimental profiles *R* (solid line). (*c*)–(*f*) Experimental profiles with reflection specimen (*R*) geometry (Fig. 2.3.1.3) with $\alpha_{\rm ES}$ 1° and $\alpha_{\rm RS}$ 0.046° (solid line profiles), and transmission specimen (*T*) (Fig. 2.3.1.12) with $\alpha_{\rm ES}$ 2° and receiving axial divergence parallel slits (dotted profiles). Cu $K\alpha$ radiation. (*a*) Si(531), (*b*) quartz(100), (*c*) Si(111), (*d*) Si(220), (*e*) Si(311), and (*f*) Si(422).

2.3.1.1.5. *Focal line and receiving-slit widths*

The projected source width F_w and receiving-slit width RS_w each add a symmetrical broadening to the profiles that is constant for all angles. Both the profile width and the intensity increase with increasing take-off angle (Section 2.3.5). However, the contribution of F_w is small when the line focus is used, Fig. 2.3.1.9(*a*). The receiving slit can easily be changed and it is one of the most important elements in controlling the profile width, intensity, and peak-to-background ratio, as is shown in Figs. 2.3.1.9(*a*) and (*c*). Because of the contributions of other broadening factors, $\alpha_{\rm RS}$ can be about twice α_F (line focus) without significant loss of resolution.

The projected width of the X-ray tube focus F_w is given in equation (2.3.1.2). The aperture is

$$\alpha_F = 2\arctan(F_w/2R). \qquad (2.3.1.8)$$

For a line focus with actual width $F'_w = 1$ mm, $\psi = 5°$, and $R = 185$ mm, $\alpha_F = 0.011°$. The receiving-slit aperture is

$$\alpha_{\rm RS} = 2\arctan(\mathrm{RS}_w/2R). \qquad (2.3.1.9)$$

For $\mathrm{RS}_w = 0.2$ mm and $R = 185$ mm. $\alpha_{\rm RS}$ is 0.062°. The FWHM of the profiles is always greater than the receiving-slit aperture because of the other broadening factors.

2.3.1.1.6. *Aberrations related to the specimen*

The major displacement errors arising from the specimen are (1) displacement of the specimen surface from the axis of rotation, (2) use of a flat rather than a curved specimen, and (3) specimen transparency. These are illustrated schematically for the focusing plane in Fig. 2.3.1.10(*a*). The rays from a highly absorbing or very thin specimen with the same curvature as the focusing circle converge at *A* without broadening and at the correct 2θ. The rays from the flat surface cause an asymmetric profile shifted to *B*. Penetration of the beam below the surface combined with the flat specimen causes additional broadening and a shift to *C*.

The most frequent and usually the largest source of angular errors arises from displacement of the specimen surface from the diffractometer axis of rotation. It is not easy to avoid and may arise from several sources. It is advisable to check the reproducibility of inserting the specimen in the diffractometer by recording an isolated peak at low 2θ for each insertion. If only a radial displacement *s* occurs, the reflection is shifted

$$\Delta 2\theta(\mathrm{rad}) = \pm 2s\cos\theta/R, \qquad (2.3.1.10)$$

where *R* is the diffractometer radius. A plot of equation (2.3.1.10) is shown in Fig. 2.3.1.10(*b*). The shift is to larger or smaller angles depending on the direction of the displacement and there is no broadening if the displacement is only radial and relatively small. Even a small displacement causes a relatively large shift; for example, if $s = +0.1$ mm and $R = 185$ mm, $\Delta 2\theta = +0.06°$ at $20°2\theta$. This gives rise to a systematic error in the recorded reflection angles, which increases with decreasing 2θ. It could be handled with a $\cos\theta\cot\theta$ plot, providing it was the only source of error. There are other possible sources of displacement such as (*a*) if the bearing surface of the specimen post was not machined to lie exactly on the axis of rotation, (*b*) improper specimen preparation or insertion in which the surface was not exactly coincident with the bearing surface or (*c*) nonplanar specimen surface, irregularities, large particle sizes, and specimen transparency. Source (*a*) leads to a constant error

Copyright © 2006 International Union of Crystallography

in all measurements, and errors due to (*b*) and (*c*) vary with each specimen.

Ideally, the specimen should be in the form of a focusing torus because of the beam divergence in the equatorial and axial planes. The curvatures would have to vary continuously and differently during the scan and it is impracticable to make specimens in such forms. An approximation is to make the specimen in a flexible cylindrical form with the radius of curvature increasing with decreasing 2θ (Ogilvie, 1963). This requires a very thin specimen (thus reducing the intensity) to avoid cracking and surface irregularities, and also introduces background from the substrate. A compromise uses rigid curved specimens, which match the SFC (Fig. 2.3.1.3) at the smallest 2θ angle to be scanned, and this eliminates most of the aberration (Parrish, 1968). A major disadvantage of the curvature is that it is not possible to spin the specimen.

In practice, a flat specimen is almost always used. The specimen surface departs from the focusing circle by an amount h at a distance $l/2$ from the specimen centre:

$$h = R_{\rm FC} - [R_{\rm FC}^2 - (l^2/2)]^{1/2}. \qquad (2.3.1.11)$$

This causes a broadening of the low-2θ side of the profile and shifts the centroid $\Delta 2\theta$ to lower 2θ:

$$\Delta 2\theta(\text{rad}) = -\alpha^2/(6\tan\theta). \qquad (2.3.1.12)$$

For $\alpha = 1^\circ$ and $2\theta = 20^\circ$, $\Delta 2\theta = -0.016^\circ$. The peak shift is about one-third as large as the centroid shift in the forward-reflection region. This aberration can be interpreted as a continuous series of specimen-surface displacements, which increase from 0 at the centre of the specimen to a maximum value at the ends. The effect increases with α and decreasing 2θ. The profile distortion is magnified in the small 2θ-angle region where the axial divergence also increases and causes similar effects. Typical flat-specimen profiles are shown in Fig. 2.3.1.10(*c*) and computed centroid shifts in Fig. 2.3.1.10(*d*).

The specimen-transparency aberration is caused by diffraction from below the surface of the specimen which asymmetrically broadens the profile (Langford & Wilson, 1962). The peak and centroid are shifted to smaller 2θ as shown in Fig. 2.3.1.10(*e*). For the case of a thick absorbing specimen, the centroid is shifted

$$\Delta 2\theta(\text{rad}) = \sin 2\theta/2\mu R \qquad (2.3.1.13)$$

and for a thin low-absorbing specimen

$$\Delta 2\theta(\text{rad}) = t\cos\theta/R, \qquad (2.3.1.14)$$

where μ is the effective linear absorption coefficient of the specimen used, t the thickness in cm, and R the diffractometer radius in cm. The intermediate absorption case is described by Wilson (1963). A plot of equation (2.3.1.13) for various values of μ is given in Fig. 2.3.1.10(*f*). The effect varies with $\sin 2\theta$ and is maximum at 90° and zero at 0° and 180°. For example, if $\mu = 50\,\text{cm}^{-1}$, the centroid shift is -0.033° at 90° and falls to -0.012° at 20°2θ.

The observed intensity is reduced by absorption of the incident and diffracted beams in the specimen. The intensity loss is $\exp(-2\mu/x_s \operatorname{cosec}\theta)$, where μ is the linear absorption coefficient of the powder sample (it is almost always smaller than the solid material) and x_s is the distance below the surface, which may be equal to the thickness in the case of a thin film or low-absorbing material specimen. The thick (1 mm) specimen of LiF in Fig. 2.3.1.10(*e*) had twice the peak intensity of the thin (0.1 mm) specimen.

The aberration can be avoided by making the sample thin. However, the amount of incident-beam intensity contributing to the reflections could then vary with θ because different amounts are transmitted through the sample and this may require corrections of the experimental data. Because the effective reflecting volume of low-absorbing specimens lies below the surface, care must be taken to avoid blocking part of the diffracted beam with the antiscatter slits or the specimen holder, particularly at small 2θ.

There are additional problems related to the specimen such as preferred orientation, particle size, and other factors; these are discussed in Section 2.3.3.

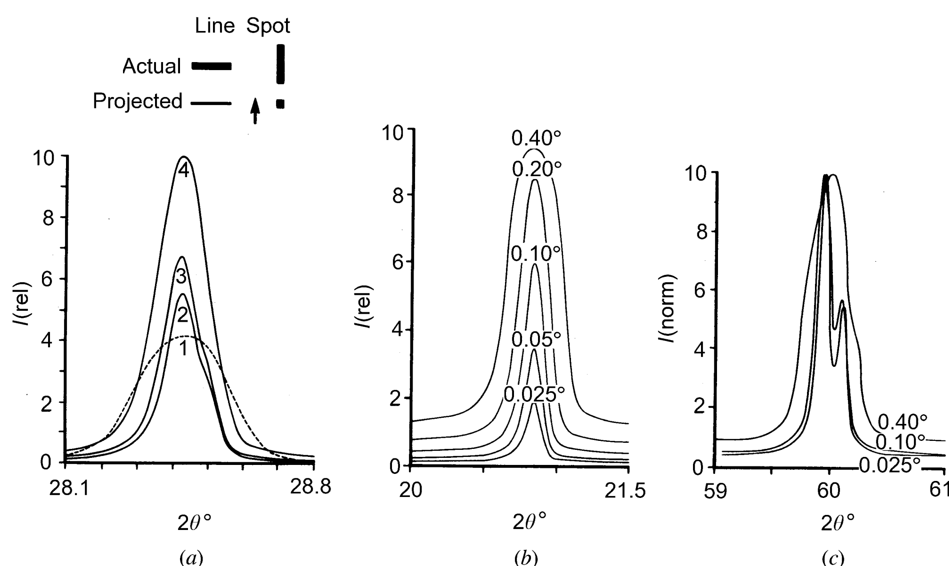

Fig. 2.3.1.9. (*a*) Effect of source size on profile shape, Cu $K\alpha$, $\alpha_{\rm ES}$ 1°, $\alpha_{\rm RS}$ 0.05°, Si(111).

No.	Projected size (mm)	FWHM (°2θ)
1	1.6 × 1.0 (spot)	0.31
2	0.32 × 10 (line)	0.11
3	0.16 × 10 (line)	0.13
4	0.32 × 12 (line)	0.17.

Effect of receiving-slit aperture $\alpha_{\rm RS}$ on profiles of quartz (*b*) (100) and (*c*) (121); peak intensities normalized, Cu $K\alpha$, $\alpha_{\rm ES}$ 1°.

references